Channel-Resilient RF Fingerprint Identification Based on Nonlinear Features with Memory Effect

Hua Fu, *Member, IEEE,* Yanfeng Sun, Linning Peng, *Member, IEEE*, Ming Liu, *Member, IEEE*

***Abstract*—Eliminating the influence of channel is crucial for radio frequency fingerprint (RFF) identification. The nonlinearity of power amplifiers (PAs) can be extracted independent of channel fading. However, when PAs exhibit memory effect, the separation of nonlinear features from channel fading becomes challenging. In this paper, based on memory polynomial PA model, an RFF nonlinear features extraction method is proposed, which includes three features containing only PA coefficients and other features mixing the PA coefficients with the training symbols. The experimental results show that when training with data received from one location and testing with data received from three other locations, the average identification accuracy can reach up to 92.92% using twenty-two IEEE 802.11 devices.**

***Index Terms*—Radio frequency fingerprint, power amplifier nonlinearity, multipath fading.**

I. Introduction

THE radio frequency fingerprint (RFF) identification is a promising physical layer authentication technique for Internet of Things (IoT). Different radio frequency (RF) components, including crystal oscillator, mixer, filter and power amplifier (PA), bring various types of RFF features such as carrier frequency offset (CFO), frequency distortion, and nonlinearity. However, CFO has been shown to be time-varying [1]. Moreover, the distortion caused by the imperfect filter is mixed with the multipath channel fading, making it difficult to extract for wideband signals.

Nonlinear PA is widely used in the RF front-end. It provides high power efficiency but introduces nonlinear distortion in the signal. The nonlinearity characteristics can be used as RFF. However, channel fading has an impact on the classification performance of nonlinear features. The spectral regrowth features have been analyzed based on the complex power-series PA model in [2]. The experimental results show that the classification error rate increases to 0.48 when the IEEE 802.15.4 sensors are trained and tested at different locations. The paper [3] considers the memoryless Bessel-Fourier PA model and uses a distorted constellation diagram as the feature to identify eight PAs. The classification performance is significantly degraded when the training and testing are performed with different channels. In fact, due to the differences in the nature of nonlinearity and propagation channel, the nonlinear features can be separated from the channel effect which is a linear process in general. An iterative algorithm has been proposed in [4] to separately estimate the nonlinearity and channel coefficients, where the behavior of PA is modeled by the memoryless power series. The identification performance has been tested in the orthogonal frequency-division multiplexing (OFDM) system using simulated PA models.

Although many existing works used memoryless nonlinear models to characterize the PA behavior, the memory effect in real PAs often arises due to thermal effects [5], [6]. This implies that the AM/AM and AM/PM functions are not static, but rather dynamic and dependent on the previous input levels. The memory effect of the PA makes it difficult to separate the nonlinear features and channel effects.

A few works in the literature also studied the RFF identification for IEEE 802.11 devices with channel effects mitigation. In [7], [8], the received signal was first equalized to remove the channel effect. Consequently, the frequency offset was restored to the equalized signal and was leveraged as the RFF feature. In [9], a time domain least mean square equalization-based RFF feature extraction method was proposed. It achieves accurate identification performance when the training and testing data have similar channels. Nelder-Mead simplex channel estimation algorithm is proposed in [10] for multipath channel of a known number of paths. The simulation results demonstrate the impact of channel length on RFF classification performance. The related parameters are optimized in [11].

In this paper, we propose to extract channel-resilient nonlinear RFF features based on the memory polynomial PA model. This model can be considered as a truncation of the general Volterra series [5]. The main contributions of this paper are listed as follows:

- By expressing the signals in matrix form and rearranging the elements of the matrix, the expressions of the PA-channel mixed coefficients are derived. These coefficients are then estimated using the least squares (LS) method.
- Three nonlinear features that contain only PA contribution can be found based on the PA-channel mixed coefficients. By summing and dividing the received training sequences with different lengths, more nonlinear RFF features that are combinations of the PA coefficients and the training symbols can be obtained.
- The identification performance of the proposed nonlinear RFF features is tested using 22 IEEE 802.11 devices. The average accuracy can reach up to 92.92% when training

This work was supported in part by National Key Research and Development Program of China under Grant 2022YFB4300300, and National Natural Science Foundation of China under Grant 62001106, 62171120 and 61971029.

H. Fu, Y. Sun, and L. Peng are with the School of Cyber Science and Engineering, Southeast University, Nanjing 210096, China. H. Fu and L. Peng are also with the Purple Mountain Laboratories for Network and Communication Security, Nanjing 211111, China. (e-mail: hfu@seu.edu.cn; 1091282902@qq.com; pengln@seu.edu.cn)

M. Liu is with the Engineering Research Center of Network Management Technology for High-Speed Railway of Ministry of Education, School of Computer and Information Technology, Beijing Jiaotong University, Beijing 100044, China. (e-mail: mingliu@bjtu.edu.cn)

with data received from only one location and testing with data received from three other locations.

The remainder of this paper is organized as follows. In Section II, the PA model is introduced and the received signal is derived with nonlinearity and channel effects. In Section III, the RFF extraction method is proposed. The experimental system and identification results are presented in Section IV. Section V concludes the paper.

II. System Model

A. PA model based on memory polynomial

Memory polynomials can be used to model the asymmetry and dynamic AM/AM and AM/PM functions. Only odd-order nonlinear terms are considered in this model, because the even-order terms are removed by the bandpass filter. The equivalent discrete baseband PA model can be expressed as [5]

$$x\left[n\right]=\sum_{k=0}^{K}\sum_{m=0}^{M}f_{2k+1,m}|d\left[n-m\right]|^{2k}d\left[n-m\right] \tag{1}$$

where $d[n]$ is the discrete input signal of PA, $x[n]$ is the discrete output signal. $f_{2k+1,m}$ is the Volterra kernel of the PA, the nonlinearity order is up to $2K+1$ and M is the memory length of PA model.

Denote the length of input signal $d[n]$ as N. The output signal $x[n]$ can be rewritten in matrix form as

$$\mathbf{x}=\mathbf{D}_N^{(M)}\mathbf{f} \tag{2}$$

where $\mathbf{x}\in\mathbb{C}^{(N+M)\times 1}$ and the input signal matrix $\mathbf{D}_N^{(M)}\in\mathbb{C}^{(N+M)\times(K+1)(M+1)}$ is

$$\mathbf{D}_N^{(M)}=\begin{bmatrix}\mathbf{d}_1 & \mathbf{0} & \cdots & \mathbf{0}\\ \mathbf{d}_2 & \mathbf{d}_1 & \cdots & \mathbf{0}\\ \vdots & \vdots & \ddots & \vdots\\ \mathbf{d}_N & \mathbf{d}_{N-1} & \cdots & \mathbf{d}_{N-M}\\ \mathbf{0} & \mathbf{d}_N & \vdots & \vdots\\ \vdots & \vdots & \ddots & \mathbf{d}_{N-1}\\ \mathbf{0} & \mathbf{0} & \mathbf{0} & \mathbf{d}_N\end{bmatrix} \tag{3}$$

with $\mathbf{d}_n\in\mathbb{C}^{1\times(K+1)}$ and

$$\mathbf{d}_n=\left[d\left[n\right],\ |d\left[n\right]|^2d\left[n\right],\ \cdots,\ |d\left[n\right]|^{2K}d\left[n\right]\right]. \tag{4}$$

The Volterra kernel vector $\mathbf{f}\in\mathbb{C}^{(K+1)(M+1)\times 1}$ is written as

$$\mathbf{f}=\left[\mathbf{f}_0,\cdots,\mathbf{f}_M\right]^T \tag{5}$$

with

$$\mathbf{f}_m=[f_{1,m},\ f_{3,m},\ \cdots,\ f_{2K+1,m}]. \tag{6}$$

B. Received signal

At the receiver side, the received signal is first synchronized and down-converted to the baseband. The resulting baseband signal can be seen as being distorted by a baseband equivalent channel [4]. In particular, the received baseband signal can be written as

$$y\left[n\right]=\sum_{l_h=1}^{L_h}h_{l_h}x[n-l_h+1]+n_{\mathrm{A}}[n] \tag{7}$$

where h_{l_h} is the discrete channel impulse response, L_h is the length of channel response, and n_{A} represents the complex baseband noise which follows circular symmetric Gaussian distribution with zero mean and variation of σ_n^2, i.e. $n_{\mathrm{A}}\sim\mathcal{CN}\left(0,\sigma_n^2\right)$.

The received baseband signal can also be rewritten in matrix format, such that

$$\mathbf{y}=\mathbf{H}\mathbf{x}+\mathbf{n}_{\mathrm{A}} \tag{8}$$

where $\mathbf{y}\in\mathbb{C}^{(N+M+L_h-1)\times 1}$, $\mathbf{H}\in\mathbb{C}^{(N+M+L_h-1)\times(N+M)}$ is the channel matrix with

$$\mathbf{H}=\begin{bmatrix}h_1 & 0 & \cdots & 0\\ h_2 & h_1 & \cdots & 0\\ \vdots & \vdots & \ddots & \vdots\\ h_{L_h} & h_{L_h-1} & \cdots & \vdots\\ 0 & h_{L_h} & \vdots & h_1\\ \vdots & \vdots & \vdots & \vdots\\ 0 & 0 & 0 & h_{L_h}\end{bmatrix}, \tag{9}$$

and $\mathbf{n}_A\in\mathbb{C}^{(N+M+L_h-1)\times 1}$ is the noise vector.

Based on (1) and (7), the received baseband signal $y[n]$ can be written as

$$\begin{aligned}y[n]=&\sum_{l_h=1}^{L_h}\sum_{k=0}^{K}\sum_{m=0}^{M}h_{l_h}f_{2k+1,m}\left|d\left[n-m-l_h+1\right]\right|^{2k}\\&\cdot d\left[n-m-l_h+1\right]+n_{\mathrm{A}}[n].\end{aligned} \tag{10}$$

Combining (2) and (8) and rearranging $\mathbf{H}$, we have

$$\begin{aligned}\mathbf{y}&=\mathbf{H}\mathbf{D}_N^{(M)}\mathbf{f}+\mathbf{n}_{\mathrm{A}}\\&=\mathbf{D}_N^{(M+L_h-1)}\widehat{\mathbf{H}}\mathbf{f}+\mathbf{n}_{\mathrm{A}}=\mathbf{D}_N^{(M+L_h-1)}\widehat{\mathbf{f}}+\mathbf{n}_{\mathrm{A}}\end{aligned} \tag{11}$$

where $\mathbf{D}_N^{(M+L_h-1)}\in\mathbb{C}^{(N+M+L_h-1)\times(K+1)(M+L_h)}$, the construction method of $\mathbf{D}_N^{(M+L_h-1)}$ is the same as that of $\mathbf{D}_N^{(M)}$ in (3). $\widehat{\mathbf{H}}\in\mathbb{C}^{(K+1)(M+L_h)\times(K+1)(M+1)}$ is composed of $\mathbf{H}_{l_h}, l_h\in\{1\cdots L_h\}$ with $\mathbf{H}_{l_h}\in\mathbb{C}^{K+1}$ is a diagonal matrix such that

$$\mathbf{H}_{l_h}=\begin{bmatrix}h_{l_h} & & \mathbf{0}\\ & \ddots & \\ \mathbf{0} & & h_{l_h}\end{bmatrix}. \tag{12}$$

The arrangement of $\mathbf{H}_{l_h}$ in $\widehat{\mathbf{H}}$ is the same as the arrangement of h_{l_h} in $\mathbf{H}$, with the other positions filled with 0. $\widehat{\mathbf{f}}\in\mathbb{C}^{(K+1)(M+L_h)\times 1}$ and $\widehat{\mathbf{f}}=\widehat{\mathbf{H}}\mathbf{f}$. Hence, $\widehat{\mathbf{f}}$ is written as

$$\begin{aligned}\widehat{\mathbf{f}}=\big[&h_1f_{1,0}\quad\cdots\quad h_1f_{2K+1,0}\quad h_2f_{1,0}+h_1f_{1,1}\quad\cdots\\&h_2f_{2K+1,0}+h_1f_{2K+1,1}\quad h_3f_{1,0}+h_2f_{1,1}+h_1f_{1,2}\\&\cdots\quad h_{L_h}f_{2K+1,M-1}+h_{L_h-1}f_{2K+1,M}\quad h_{L_h}f_{1,M}\\&\cdots\quad h_{L_h}f_{2K+1,M}\big]^T.\end{aligned} \tag{13}$$

It can be seen from (13) that except for the first and the last $K+1$ terms which only involve one channel coefficient multiplied by the PA coefficient, the other terms are sums of multiple products, making it difficult to directly solve the PA coefficients $f_{2k+1,m}$. In the next section, a new RFF feature extraction scheme is proposed, where the features are in function of $f_{2k+1,m}$ and the influence of the channel is removed.

III. The Proposed RFF Extraction Scheme

A. Nonlinear coefficients acquisition

We first estimate $\widehat{\mathbf{f}}$ using (11). To this end, the matrix $\mathbf{D}_N^{(M+L_h-1)}$ needs to be constructed properly. Hence, the value of nonlinearity order $2K+1$ and the equivalent memory length $M+L_h-1$ need to be determined. However, when the nonlinearity order increases, the influence of the nonlinearity decreases proportionally and becomes negligible [6]. Without loss of generality, in this paper the maximum nonlinearity order is set to 3, i.e. $K=1$ [5]. Then, to estimate the value of $M+L_h-1$, we first assume that $M+L_h-1$ is in the range of $[R_{min}, R_{max}]$. For any value $R \in [R_{min}, R_{max}]$, $\mathbf{D}_{N_p}^{(R)}$ can be constructed using the known training sequence $d[n], n \in \{1, \cdots, N_p\}$ through (3), where N_p is the length of the preamble part of the signal. The matrix consisting of the first N_p rows of $\mathbf{D}_{N_p}^{(R)}$ is denoted as $\tilde{\mathbf{D}}_{N_p}^{(R)}$. Then the corresponding estimate of $\widehat{\mathbf{f}}$, denoted as $\bar{\mathbf{f}}_R$, can be computed by the LS method, such that

$$\bar{\mathbf{f}}_R = \tilde{\mathbf{D}}_{N_p}^{(R)\dagger} \bar{\mathbf{y}}_{(N_p)} \tag{14}$$

where the superscript $(\cdot)^\dagger$ denotes the pseudoinverse of the matrix, $\bar{\mathbf{y}}_{(N_p)}$ denotes the preamble part of the received signal after synchronization and CFO compensation [7], [9].

We note that for $K=1$, the odd terms of $\widehat{\mathbf{f}}$ contain Volterra kernels with $k=0$, and the even terms contain that with $k=1$. The ratio between their sums is independent of the channel response, such that

$$\begin{aligned} \tau_{oe} &= \frac{\sum_{i=0}^{M+L_h-1} \widehat{\mathbf{f}}(2i+1)}{\sum_{i=1}^{M+L_h} \widehat{\mathbf{f}}(2i)} \\ &= \frac{\sum_{m=0}^{M} f_{1,m} \sum_{l_h=1}^{L_h} h_{l_h}}{\sum_{m=0}^{M} f_{3,m} \sum_{l_h=1}^{L_h} h_{l_h}} = \frac{\sum_{m=0}^{M} f_{1,m}}{\sum_{m=0}^{M} f_{3,m}}. \end{aligned} \tag{15}$$

For each estimate $\bar{\mathbf{f}}_R$, the corresponding ratio τ_{oe} is denoted as $\tau_{oe,R}$. We note that when $R \geq M+L_h-1$, the value of $\tau_{oe,R}$ tends to be stable. Therefore, we calculate the variance of sequence $[\tau_{oe,R}, \cdots, \tau_{oe,R+4}]$ in turn, as shown in Fig. 1. To detect the starting point where the variance reaches stability, we note that this starting point is a valley in the variance curve. Hence, we first identify all the valleys in the variance curve. We use the maximum value of variance to subtract the value of variance to transform the valleys in the curve into peaks. Then these peaks can be detected using the *findpeaks* function in MATLAB. Because the value of variance still has slight fluctuation after reaching stability, multiple valleys may also be detected in the stable region of the variance. We choose the first valley value that satisfies the conditions of being less than twice the minimum value of variance and the sum of the valley value and the following two points being less than 10 times the minimum value of the variance as the value of L_M, as shown by the cross marks in Fig. 1. Furthermore, for all devices, the maximum value of L_M is limited to 24. The corresponding $\bar{\mathbf{f}}_{L_M}$ is selected as the estimate of $\widehat{\mathbf{f}}$.

B. Channel-resilient nonlinear features

With the nonlinear coefficient estimation $\widehat{\mathbf{f}}$ available, we propose a new method to extract the nonlinear features.

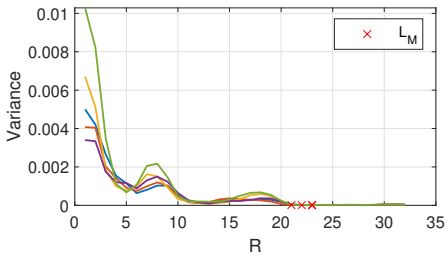

Fig. 1. Variance of sequence $[\tau_{oe,R}, \cdots, \tau_{oe,R+4}]$ in function of R.

First of all, the nonlinear features ϕ_1 and ϕ_2 can be obtained by calculating the ratios of the first two terms and the last two terms of $\widehat{\mathbf{f}}$, respectively, such that

$$\phi_1 = \frac{\widehat{\mathbf{f}}(1)}{\widehat{\mathbf{f}}(2)} = \frac{h_1 f_{1,0}}{h_1 f_{3,0}} = \frac{f_{1,0}}{f_{3,0}}, \tag{16}$$

$$\phi_2 = \frac{\widehat{\mathbf{f}}((K+1)(M+L_h)-1)}{\widehat{\mathbf{f}}((K+1)(M+L_h))} = \frac{h_{L_h} f_{1,M}}{h_{L_h} f_{3,M}} = \frac{f_{1,M}}{f_{3,M}}. \tag{17}$$

Moreover, τ_{oe} in (15) also contains only PA coefficients, hence can be considered as a nonlinear feature ϕ_3, such that

$$\phi_3 = \tau_{oe} = \frac{\sum_{i=0}^{M+L_h-1} \widehat{\mathbf{f}}(2i+1)}{\sum_{i=1}^{M+L_h} \widehat{\mathbf{f}}(2i)} = \frac{\sum_{m=0}^{M} f_{1,m}}{\sum_{m=0}^{M} f_{3,m}}. \tag{18}$$

On the other hand, according to (7) and ignoring noise, the sum of the elements of $\mathbf{y}$ can be expressed as

$$\sum_{n=1}^{N+M+L_h-1} y[n] = \sum_{l_h=1}^{L_h} h_{l_h} \sum_{n=1}^{N+M} x[n]. \tag{19}$$

Similarly, according to (1), the sum of the elements of $\mathbf{x}$ can be expressed as

$$\sum_{n=1}^{N+M} x[n] = \sum_{k=0}^{K} \sum_{m=0}^{M} f_{2k+1,m} \sum_{n=1}^{N} |d[n]|^{2k} d[n]. \tag{20}$$

Substituting (20) into (19), we have

$$\sum_{n=1}^{N+M+L_h-1} y[n] = \sum_{l_h=1}^{L_h} h_{l_h} \sum_{k=0}^{K} \sum_{m=0}^{M} f_{2k+1,m} \sum_{n=1}^{N} |d[n]|^{2k} d[n]. \tag{21}$$

We note that in (21), the sum of channel coefficients $\sum_{l_h=1}^{L_h} h_{l_h}$ becomes a common factor when summing up $y[n]$ with different lengths. Hence, the impact of channel can be eliminated by calculating their ratio. More importantly, when the values of $d[n]$ are known, the ratio of the sums of $y[n]$ with different lengths is only determined by $f_{2k+1,m}$'s and can be considered as a representation of nonlinear features. Therefore, we choose $d[n]$ from the known training sequence. Since the multipath fading may cause inter-symbol interference, the first N_1 samples of the received training sequence are discarded. Hence, the corresponding $d[n]$ can be expressed as $d[n], n \in \{N_1+1, \cdots, N_2\}, N_1+L_M+1 \leq N_2 \leq N_p$. Denoting the selected $d[n], n \in \{N_1+1, \cdots, N_2\}$ sequence as

$d'[n], n \in \{1, \cdots, N_2 - N_1\}$, the sum of $y[n]$ can be written as

$$\begin{aligned} S_{N_1,N_2} &= \sum_{l_h=1}^{L_h} h_{l_h} \sum_{k=0}^{K} \sum_{m=0}^{M} f_{2k+1,m} \sum_{n=N_1+1}^{N_2} |d[n]|^{2k} d[n] \\ &= \sum \left(\mathbf{D}'^{(M+L_h-1)}_{N_2-N_1} \widehat{\mathbf{f}} \right) \\ &= \sum \left(\tilde{\mathbf{D}}'^{(M+L_h-1)}_{N_2-N_1} \widehat{\mathbf{f}} \right) + \sum \left(\ddot{\mathbf{D}}'^{(M+L_h-1)}_{N_2-N_1} \widehat{\mathbf{f}} \right) \\ &= \sum_{n=N_1+1}^{N_2} y[n] - \sum \left(\ddot{\mathbf{D}}^{(M+L_h-1)}_{N_1} \widehat{\mathbf{f}} \right) + \sum \left(\ddot{\mathbf{D}}'^{(M+L_h-1)}_{N_2-N_1} \widehat{\mathbf{f}} \right) \\ &= \sum_{n=N_1+1}^{N_2} y[n] + \sum \left(\ddot{\mathbf{D}}'^{(M+L_h-1)}_{N_2-N_1} \widehat{\mathbf{f}} - \ddot{\mathbf{D}}^{(M+L_h-1)}_{N_1} \widehat{\mathbf{f}} \right) \end{aligned} \tag{22}$$

where $\mathbf{D}'^{(M+L_h-1)}_{N_2-N_1}$ can be constructed through (3) using $d'[n], n \in \{1, \cdots, N_2 - N_1\}$. The matrix consisting of the first $N_2 - N_1$ rows of $\mathbf{D}'^{(M+L_h-1)}_{N_2-N_1}$ is denoted as $\tilde{\mathbf{D}}'^{(M+L_h-1)}_{N_2-N_1}$ and that consisting of the last $M + L_h - 1$ rows is denoted as $\ddot{\mathbf{D}}'^{(M+L_h-1)}_{N_2-N_1}$. $\mathbf{D}^{(M+L_h-1)}_{N_1}$ is constructed through (3) using $d[n], n \in \{1, \cdots, N_1\}$. The matrix consisting of the last $M + L_h - 1$ rows of $\mathbf{D}^{(M+L_h-1)}_{N_1}$ is denoted as $\ddot{\mathbf{D}}^{(M+L_h-1)}_{N_1}$. $\sum(\cdot)$ means summing up all the elements in the vector.

Therefore, the nonlinear feature can be defined as

$$\begin{aligned} \phi_{\frac{N_1,N_2}{N_3,N_4}} &= \frac{S_{N_1,N_2}}{S_{N_3,N_4}} \\ &= \frac{\sum_{k=0}^{K} \sum_{m=0}^{M} f_{2k+1,m} \sum_{n=N_1+1}^{N_2} |d[n]|^{2k} d[n]}{\sum_{k=0}^{K} \sum_{m=0}^{M} f_{2k+1,m} \sum_{n=N_3+1}^{N_4} |d[n]|^{2k} d[n]} \\ &= \frac{\sum_{n=N_1+1}^{N_2} y[n] + \sum \left(\ddot{\mathbf{D}}'^{(M+L_h-1)}_{N_2-N_1} \widehat{\mathbf{f}} - \ddot{\mathbf{D}}^{(M+L_h-1)}_{N_1} \widehat{\mathbf{f}} \right)}{\sum_{n=N_3+1}^{N_4} y[n] + \sum \left(\ddot{\mathbf{D}}'^{(M+L_h-1)}_{N_4-N_3} \widehat{\mathbf{f}} - \ddot{\mathbf{D}}^{(M+L_h-1)}_{N_3} \widehat{\mathbf{f}} \right)}. \end{aligned} \tag{23}$$

For $(N_1, N_2) \neq (N_3, N_4)$, $\phi_{\frac{N_1,N_2}{N_3,N_4}}$ can be regarded as a weighted mixture of $f_{2k+1,m}$. When the values of $d[n]$ are known, $\phi_{\frac{N_1,N_2}{N_3,N_4}}$ depends only on the values of $f_{2k+1,m}$. Hence, different combinations of (N_1, N_2) and (N_3, N_4) can lead to various $\phi_{\frac{N_1,N_2}{N_3,N_4}}$ features. We note that if the preamble is composed of periodic symbols, we need to ensure that $\frac{\sum_{n=N_1+1}^{N_2} d[n]}{\sum_{n=N_3+1}^{N_4} d[n]} \neq \frac{\sum_{n=N_1+1}^{N_2} |d[n]|^2 d[n]}{\sum_{n=N_3+1}^{N_4} |d[n]|^2 d[n]}$ when selecting the values of (N_1, N_2) and (N_3, N_4). Otherwise, $\phi_{\frac{N_1,N_2}{N_3,N_4}}$ becomes a constant and loses the feature.

IV. Experimental Results

A. Experimental system

An experimental system has been set up using a universal software radio peripheral (USRP) N210 as the receiver and 21 Wi-Fi access point (AP) routers, including 15 MERCURY™ MW305R and 6 D-Link™ DWL-2000AP+A. One mobile phone Honor™ 6 is used to communicate with the AP routers to trigger the transmission of OFDM data frames, which is also considered as an IEEE 802.11 device. Hence, the total number of devices to be identified is 22. The experiment is conducted in an $8.8\ \mathrm{m} \times 8.8\ \mathrm{m}$ room, with the AP routers placed in fixed positions at the corner. The receiver is moved to four different locations to receive the signals with different channels. The LS estimations of channel frequency responses [10] are depicted in Fig. 2 for the same AP router. Because both the device and receiver remain the same, the differences of the channel responses in different receiving positions come from the location-dependent channel fading. At each position, we collected approximately 1000 frames for each AP router. The signal power is normalized for each frame. The average signal-to-noise ratio (SNR) of the collected data is 36.3 dB.

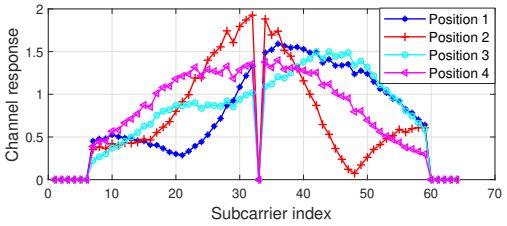

Fig. 2. Examples of normalised channel frequency responses associated to four reception positions.

TABLE I
RFF FEATURES

ϕ	$\phi_{\frac{33,160}{33,320}}$	$\phi_{\frac{33,160}{33,256}}$	$\phi_{\frac{33,192}{33,256}}$	$\phi_{\frac{33,224}{33,320}}$	$\phi_{\frac{33,256}{33,320}}$
$\phi_{\frac{33,256}{33,224}}$	$\phi_{\frac{33,160}{33,192}}$	$\phi_{\frac{33,160}{65,288}}$	$\phi_{\frac{33,192}{65,288}}$	$\phi_{\frac{65,160}{33,192}}$	$\phi_{\frac{65,160}{65,224}}$
$\phi_{\frac{65,192}{33,224}}$	$\phi_{\frac{33,88}{33,192}}$	$\phi_{\frac{33,104}{33,160}}$	$\phi_{\frac{33,104}{33,256}}$	$\phi_{\frac{33,120}{33,320}}$	$\phi_{\frac{33,136}{33,256}}$
$\phi_{\frac{33,136}{33,320}}$					

The received signal frames are synchronized and the CFO is compensated before nonlinear feature extraction. The preamble part of the IEEE 802.11 signal includes short training symbol (STS) part and long training symbol (LTS) part. The STS part consists of 10 STSs, with a length of 160 samples. The LTS part consists of a guard interval and 2 LTSs, also with a length of 160 samples. Hence, the total length of the preamble part is 320 samples. The sequences used for feature $\phi_{\frac{N_1,N_2}{N_3,N_4}}$ extraction are chosen within the preamble part of the signal. Considering the use of complete or half training symbol, 21 RFF features can be extracted as listed in Table I.

The nonlinear features extracted from 200 signal frames of 2 APs are displayed in Fig. 3 for 2 receiving locations. Different features are represented in different colors. It can be observed that the feature values extracted from different frames are very stable, forming a small cluster for each feature. Moreover, we note that figures (a) and (b), as well as figures (c) and (d), exhibit high similarity, thus proving that the proposed nonlinear features are channel-resilient. Additionally, there are significant differences among the features in figures (a) and (c), proving that the nonlinear features have good discriminability.

B. Identification performance

Convolutional neural network (CNN) has been widely used for RFF identification [7], [9]. The complex features are split into real and imaginary parts, which are then used as the input

This article has been accepted for publication in IEEE Communications Letters. This is the author's version which has not been fully edited and content may change prior to final publication. Citation information: DOI 10.1109/LCOMM.2024.3364494

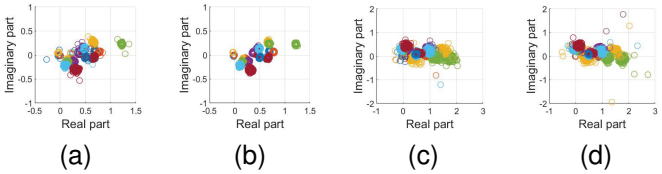

Fig. 3. 21 RFF features extracted from 200 signal frames of 2 D-Link^{TM} APs, with the receiver at Position 1 for (a) (c) and Position 2 for (b) (d).

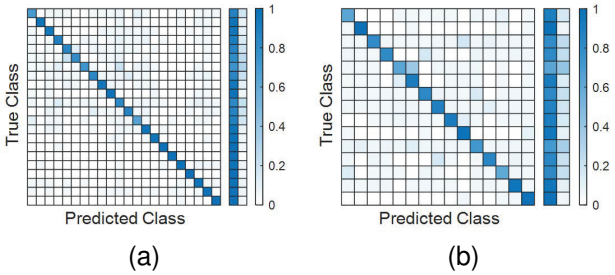

Fig. 4. Examples of confusion matrix for 1P train scenario with (a) 22 devices (b) 15 Mercury APs, the average SNR of each device is 35 dB.

for the CNN. In this paper, we use the CNN model proposed in [9], because it has a small kernel size and fast training speed. It is composed of four 1-dimensional convolution layers with 16, 32, 48 and 64 convolution kernels, respectively. The kernel size is 1×2.

To validate the channel-resilience of the nonlinear features, we use the features extracted from the data of one location as the training dataset, and test it using the features extracted from the data of three other locations, referred to 1P train. To test the impact of the number of training locations used, we also use the features extracted from the data of three locations as the training dataset, and test it using the features extracted from the data of the remaining location, referred to 3P train. The classification performance using only the 15 Mercury APs refers to the curves with '15d'. The average SNR of each device is rearranged by adding Gaussian noise. Examples of confusion matrix are presented in Fig. 4 for 1P train scenario. For Fig. 4(a), 2 Mercury APs have an accuracy of less than 80%, with a minimum accuracy of 73.31%. For Fig. 4(b), 3 APs have an accuracy of less than 80%, with a minimum accuracy of 61.78%. When the training and testing are repeated 10 times, the average classification results are presented in Fig. 5. For 1P train scenario with average SNR of 35 dB, the average accuracy is 92.92% for 22 devices and 84.59% for 15 Mercury APs. For comparison purposes, the frequency domain equalized signal with rebuilt CFO [7], referred to as FDE feature, is also tested. It can be seen that when using nonlinear features, the results are close for 1P train and 3P train scenarios. This proves that the nonlinear features are channel-resilient. Moreover, the nonlinear features outperform the FDE features at high SNR. However, the nonlinear features are relatively subtle, which affects the classification performance at low SNR regime.

V. Conclusions

In this paper, an RFF nonlinear features extraction method is proposed based on the nonlinear PA model with memory effect. The nonlinear features include three features containing only PA coefficients and other features mixing the PA coefficients with the training symbols. Experimental results show that the proposed nonlinear features can reach an average accuracy of 92.92% when training with data received from one location and testing with data received from three other locations. Hence, the proposed nonlinear features mitigate the impact of wireless channel.

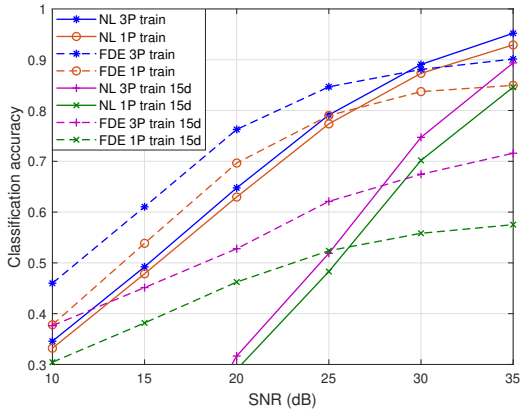

Fig. 5. Classification performance using the data of one location for training ('1P') and three locations for training ('3P').

References

[1] C. G. Wheeler and D. R. Reising, "Assessment of the impact of CFO on RF-DNA fingerprint classification performance," in *2017 Int. Conf. Comput. Netw. Commun. (ICNC)*, 2017, pp. 110–114.

[2] W. Wang, Z. Sun, S. Piao, B. Zhu, and K. Ren, "Wireless physical-layer identification: Modeling and validation," *IEEE Trans. Inf. Forensics Security*, vol. 11, no. 9, pp. 2091–2106, Sep. 2016.

[3] Y. Li, Y. Ding, J. Zhang, G. Goussetis, and S. K. Podilchak, "Radio frequency fingerprinting exploiting non-linear memory effect," *IEEE Trans. Cogn. Commun. Netw.*, vol. 8, no. 4, pp. 1618–1631, Dec. 2022.

[4] M.-W. Liu and J. F. Doherty, "Nonlinearity estimation for specific emitter identification in multipath channels," *IEEE Trans. Inf. Forensics Security*, vol. 6, no. 3, pp. 1076–1085, Sep. 2011.

[5] H. Ku and J. Kenney, "Behavioral modeling of nonlinear RF power amplifiers considering memory effects," *IEEE Trans. Microwave Theory Tech.*, vol. 51, no. 12, pp. 2495–2504, Dec. 2003.

[6] H. Ku, "Behavior modeling of nonlinear RF power amplifiers for digital wireless communication systems with implications for predistortion linearization systems," Ph.D. dissertation, Georgia Institute of Technology, USA, Oct. 2003.

[7] K. Sankhe, M. Belgiovine, F. Zhou, L. Angioloni, F. Restuccia, S. D'Oro, T. Melodia, S. Ioannidis, and K. Chowdhury, "No radio left behind: Radio fingerprinting through deep learning of physical-layer hardware impairments," *IEEE Trans. Cogn. Commun. Netw.*, vol. 6, no. 1, pp. 165–178, Mar. 2020.

[8] T. Jian, B. C. Rendon, E. Ojuba, N. Soltani, Z. Wang, K. Sankhe, A. Gritsenko, J. Dy, K. Chowdhury, and S. Ioannidis, "Deep learning for RF fingerprinting: A massive experimental study," *IEEE Internet Things Mag.*, vol. 3, no. 1, pp. 50–57, Mar. 2020.

[9] H. Fu, L. Peng, M. Liu, and A. Hu, "Deep learning based RF fingerprint identification with channel effects mitigation," *IEEE Open J. Commun. Soc.*, pp. 1668–1681, Jul. 2023.

[10] M. Fadul, D. Reising, T. D. Loveless, and A. Ofoli, "Nelder-mead simplex channel estimation for the RF-DNA fingerprinting of OFDM transmitters under Rayleigh fading conditions," *IEEE Trans. Inf. Forensics Security*, vol. 16, pp. 2381–2396, Jan. 2021.

[11] M. K. M. Fadul, J. T. Willis, D. R. Reising, and T. D. Loveless, "An analysis of process parameters for the optimization of specific emitter identification under Rayleigh fading," in *Internet of Things*, A. González-Vidal, A. Mohamed Abdelgawad, E. Sabir, S. Ziegler, and L. Ladid, Eds. Cham: Springer International Publishing, 2022, pp. 277–291.